High-performance aqueous symmetric supercapacitor based on Ni$_6$MnO$_8$-MnCO$_3$ composites self-supported electrode

S. Luo[a, b], J.E. Li[a, b, *], P.F. Xu[a], X.Y. Han[b], L. Chen[b], C.G. Hu[b, *]

[a] *School of Resources, Environment and Materials, Guangxi Key Laboratory of Processing for Non-ferrous Metals and Featured Materials, Guangxi University, Nanning, Guangxi 530004, P.R. China*

[b] *Department of Applied Physics, Chongqing University, Chongqing 400044, China*

* Corresponding author.

 E-mail addresses: hucg@cqu.edu.cn (CG Hu); ljen@gxu.edu.cn (JE Li).

Contents

Fig. S1. (a, b) XPS spectra: O 1s and C 1s of NMO-2@ACC.

Fig. S2. FESEM images of NMO-2 at different magnification: (a-c) hydrothermal treatment at 80 ℃ and (d-f) 150 ℃.

Fig. S3. (a, b) EDS spectra of the NMO-2@ACC at different areas.

Fig. S4. CV and GCD curves of NMO-2@ACC within (a), (b) 0-1V and (c), (d) -0.8-0V.

Fig. S5. (a) FESEM image of NMO-2@ACC after 5000th cycles. (b) XRD patterns of before and after cycling.

Fig. S6. (a) CV curves of NMO-2@ACC symmetric SC at voltage of 0-1.8 V and (b) -0.8-1 V. (c) Corresponding areal capacitances of NMO-2@ACC symmetric SC.

Fig. S7. GCD curve of 2 NMO-2@ACC SCs in series at a current density of 8 mA cm^{-2}.

Table S1 Comparison of relative area ratio of Mn^{2+} in Mn 2p and CO$_3^{2-}$ in O 1s high-resolution XPS spectra.

Calculation

The calculation formulas we use in this paper are as follows. The areal capacitance was calculated by the CV curves using

$$C_{s,\ s} = \frac{\int I dV}{2s \cdot v \cdot \triangle V} \tag{1}$$

where $\int I dV$ represents the area of closed CV curve, the s represents the area of the electrode, ΔV and v are the potential window and scanning rate, and GCD plot using

$$C_{s,\ s} = \frac{I \cdot \Delta t}{s \cdot \Delta V} \tag{2}$$

$$C_{s,\ m} = \frac{I \cdot \Delta t}{m \cdot \Delta V} \tag{3}$$

where I, Δt and ΔV represent the discharging current and time, potential range (excluding IR drop), respectively. The s and m represent the area and mass of active material on carbon cloth, respectively.

The volumetric energy (mWh cm^{-3}) and power (mW cm^{-3}) densities of the device were calculated based on

$$E = \frac{I \cdot \int V_{(t)}\, dt}{s \cdot 3600 d} \tag{4}$$

$$P = \frac{3600 E}{t_{discharge}} \tag{5}$$

where I, d, s, $V_{(t)}$ and $t_{discharge}$ are the current, thickness, area of the ASC device, discharging voltage and the total discharging time, respectively. Both of $V_{(t)}$ and $t_{discharge}$ are taken into account for the calculation excluding the initial IR drop. And the gravimetric energy (Wh Kg^{-1}) and power (W Kg^{-1}) densities of the device were calculated based on replacing s in equation 4 with m (quality of active substances in the device).

The real (C') and imaginary capacitances (C") were calculated by the following formulas

$$C' = -\frac{z''}{2\pi f |z|^2 s} \tag{6}$$

$$C'' = \frac{z'}{2\pi f |z|^2 s} \tag{7}$$

Where the Z', Z'', Z, f, and s replace the real and imaginary parts of the complex impedance, impedance modulus, frequency, and the geometrical area of the electrode.
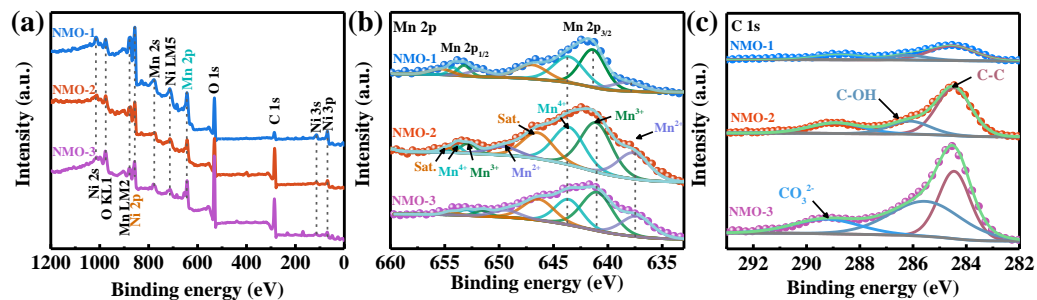

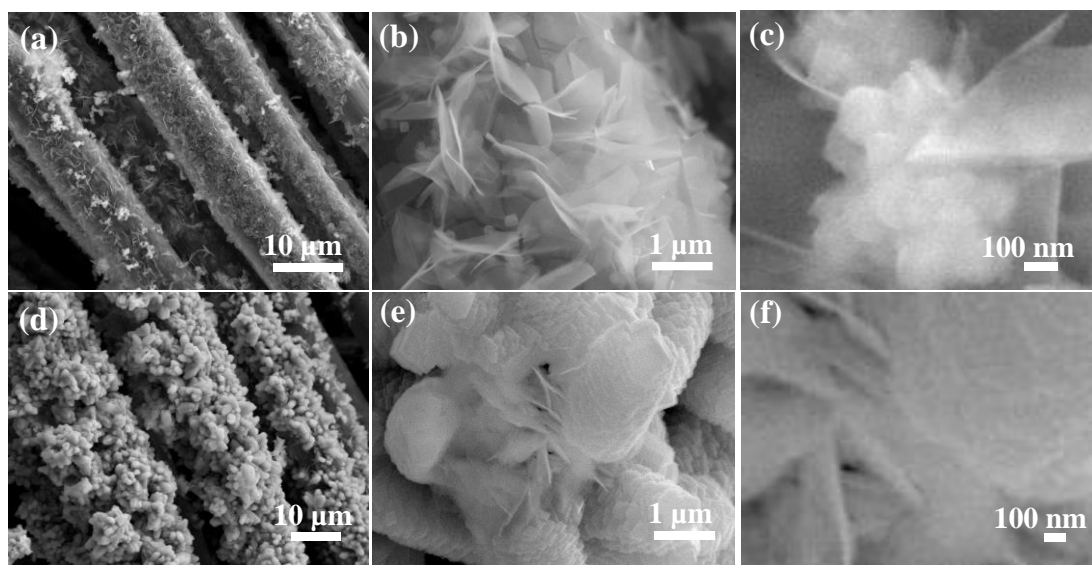**Fig. S1.** (a, b, c) XPS spectra: survey, Mn 2p and C 1s of NMO-2@ACC.

Fig. S2. FESEM images of NMO-2 at different magnification: (a-c) hydrothermal treatment at 80 °C and (d-f) 150 °C.
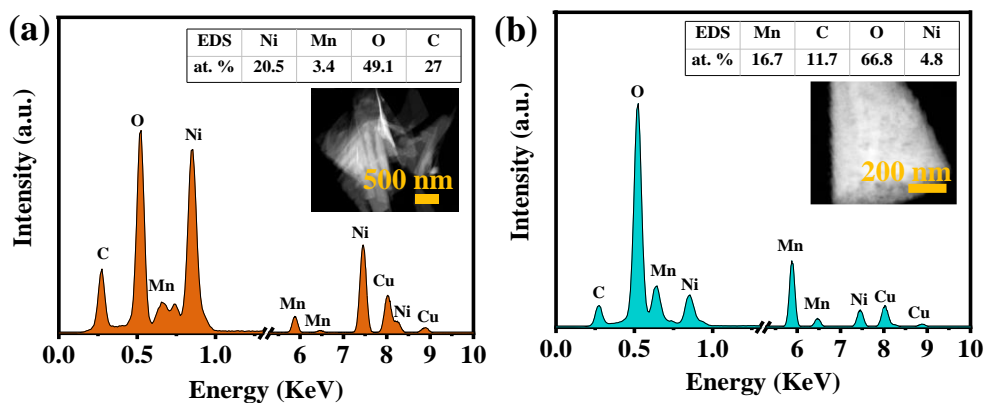
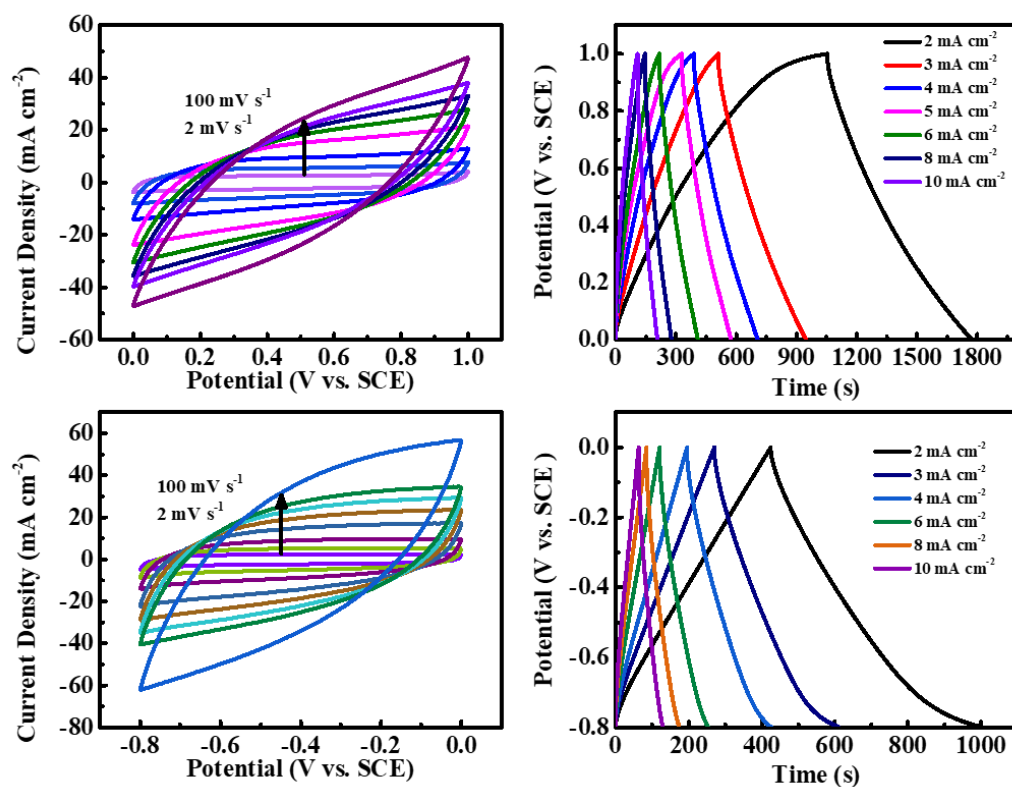**Fig. S3.** (a, b) EDS spectra of the NMO-2@ACC at different areas.

Fig. S4. CV and GCD curves of NMO-2@ACC within (a), (b) 0-1V and (c), (d) -0.8-0V.
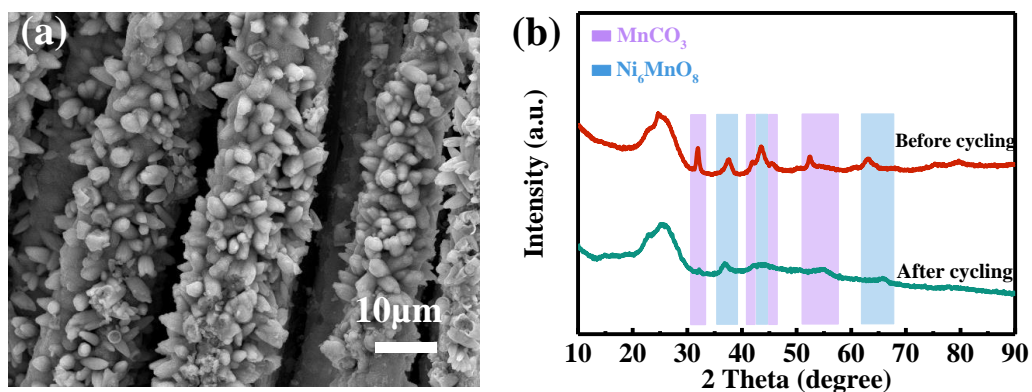
Fig. S5. (a) FESEM image of NMO-2@ACC after 5000th cycles. (b) XRD patterns of before and after cycling.
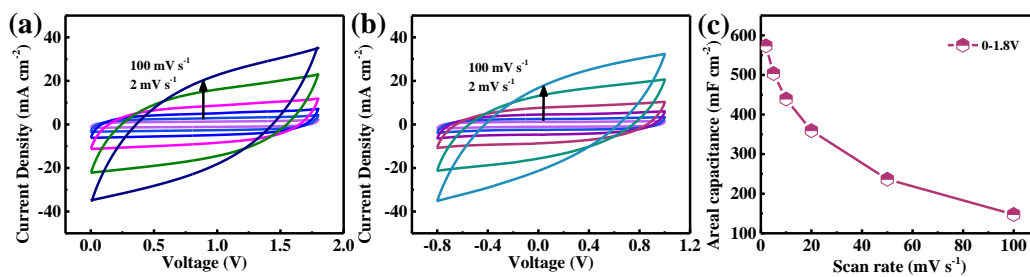

Fig. S6. (a) CV curves of NMO-2@ACC symmetric SC at voltage of 0-1.8 V and (b) -0.8-1 V. (c) Corresponding areal capacitances of NMO-2@ACC symmetric SC.
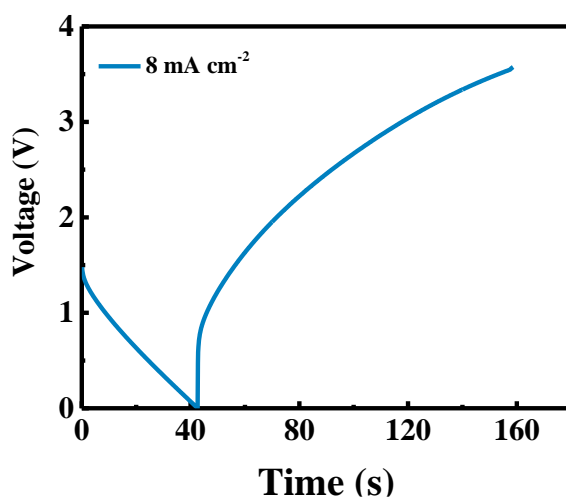

Fig. S7. GCD curve of 2 NMO-2@ACC SCs in series at a current density of 8 mA cm^{-2}.

Table S1. Comparison of relative area ratio of Mn^{2+} in Mn 2p and CO_3^{2-} in O 1s high-resolution XPS spectra. (Take the largest peak area as unit one)

Substance	NMO-1	NMO-2	NMO-3
Mn^{2+} (Mn 2p)	0.32	0.59	0.68
CO_3^{2-} (O 1s)	0.24	0.41	0.91